Check for updates

Deep space debris—Detection of potentially hazardous asteroids and objects from the southern hemisphere

Ed Kruzins[1,2]*, Lance Benner[3], Russell Boyce[1], Melrose Brown[1], David Coward[4], Sam Darwell[1], Phil Edwards[2], Lauren Elizabeth-Glina[1], Jon Giorgini[3], Shinji Horiuchi[2], Andrew Lambert[1], Joseph Lazio[3], Guifre Molera Calves[5], John Moore[4], Edwin Peters[1], Chris Phillips[2], Jamie Stevens[2] and Arie Verveer[4]

[1]University of New South Wales, Sydney, NSW, Australia, [2]Commonwealth Scientific Industrial Research Organisation, Sydney, NSW, Australia, [3]Jet Propulsion Laboratory, California Institute of Technology, Pasadena, CA, United States, [4]University of Western Australia, Perth, WA, Australia, [5]University of Tasmania, Hobart, TAS, Australia

Space debris are composed of both natural and human made objects, some in near Earth orbits while others are passing through deep space. Asteroids may represent one form of near Earth and deep space debris. In this article we report on a set of asteroid observations from the southern hemisphere. We indicate that Apollo and Aten class asteroids represent another form of deep space debris of a potentially hazardous nature to orbiting spacecraft and/or Earth based locations. We also show some of the operational challenges, types of facilities and the importance of geographic diversity, that is, necessary for detecting, observing and characterising asteroids, especially PHA's. For many years, space agencies and institutions have observed and monitored near Earth asteroids and objects (NEO's) using high gain radio frequency antennas and optical telescopes in the northern hemisphere (GSSR, Arecibo, Catalina, Pan-STARRS, Atlas and Linear) 1) However a regular operational system to monitor the southern skies does not have the same level of maturity and is where a percentage of asteroids and various human made objects are not detected until they pass into northern skies. To fill that gap the Southern Hemisphere Asteroid Radar Program (SHARP) 2) located in Australia uses available antenna time on either a 70 or 34 m beam waveguide antenna located at the Canberra Deep Space Communication Complex (CDSCC) to transmit a Doppler compensated continuous radio wave at 2.114 GHz (14.2 cm) and 7.15945 GHz (4.2 cm) toward the NEO and receive its echoes at the 64 m Parkes or 6 m × 22 m Australia Telescope Compact Array (ATCA) antennas at Narrabri in Australia. This mode of NEO observation is termed a deep space bistatic radar. The southern hemisphere program has also recently been joined by the 12 m University of Tasmania antennas at Hobart (Tasmania) and Katherine (Northern Territory). Combining SHARPS bistatic radar with small optical apertures located at the University of New South Wales (UNSW) and University of Western Australia (UWA) allows combined optical/RF NEO detections. Whilst sub-metre class optical instruments have contributed independently to asteroid detection over decades, the use of coordinated small 0.3−0.5 m instruments synchronized to large asteroid radars offers an observational flexibility and

adaptability when larger optical systems 3) are dedicated to other forms of professional optical astronomy. Since 2015, SHARP has illuminated and tracked over 30 NEO's ranging in diameter from 7 to 5000 m at ranges of 0.1–18 lunar distances (LD) from Australia.

Introduction

We often think about space debris in terms of near Earth human made objects, left over from spent rocket boosters, parts of launch fairings or spacecraft that are no longer functional or orbiting as fragments. In this article we indicate that Apollo and Aten class asteroids defined as Earth orbit crossing, represent another form of space debris from deep space. Apollo and Aten class asteroids therefore offer a potential hazard to orbiting spacecraft or Earth based locations. We show some of the operational challenges, types of facilities and the importance of geographic diversity required for detecting, observing and characterising asteroids, especially PHA's.

For many years, radar antennas in the northern hemisphere have been used to track and observe Solar System objects. Radar observations have evolved planetary science and have been applied to planetary surface research (Ostro et al., 2007). Radar has also been used to characterise water ice at the poles of Mercury (Slade et al., 1992) and polar ice surface features on Mars (Muhleman et al., 1991). Extending the range, observations have been made of the icy nature of the moons of the gas giants (Ostro and Pettengill, 1978) as well as the surface of Saturn's Moon Titan (Muhleman et al., 1990).

Extensions of planetary radar work has led to observations of near-Earth asteroids and objects (NEOs) with several clear motivations:

1. Asteroids represent primitive remnants of the early solar system and observations offer insights into their evolution and parent populations.
2. It is essential to assess the extent to which asteroids might represent a hazard to Earth infrastructures in space (satellites) and on ground.
3. Asteroids may represent targets for exploration by spacecraft.
4. Research methods developed for asteroids may be translatable to improve space situation and domain awareness of resident space objects.

Up to 2015 planetary radar work had predominantly been performed by northern hemisphere facilities such as Arecibo (Puerto Rico) and the Goldstone Solar System Radar (GSSR) which have contributed strongly to the understanding of asteroids. The addition of southern hemisphere observations such as from Australia is a next logical step. We may also add that an extension of observations to further longitudes such as the Indian sub-continent is equally logical. A wider geographical longitudinal spread as well as a southern hemisphere latitude spread, would add a wider and richer geographic diversity of observations to further refine asteroid detection datasets.

The performances of planetary radar systems was assessed by (Ostro and Giorgini, 2004; Giorgini et al., 2009; Naidu et al., 2016) indicating that geographically distributed radar facilities can reduce

uncertainties in asteroid orbit determination and increase precision in threat assessments. It was also noted (Giorgini et al., 2008; Abu Shaban. et al., 2018) that by extending radar observations to include southern hemisphere latitudes, radar facilities could:

a. Double the number of asteroids detected
b. Improve determinations of asteroid characteristics (diameter, mass, rotation and surface)
c. Improve estimates of pole directions by contiguous observation from northern to southern hemisphere (or *vice versa*).
d. Improve determination of signal-to-noise ratio variation as the asteroid transits from a northern or southern hemisphere view-point.
e. A fraction of asteroids rising from the southern hemisphere may have passed Earth by the time they can be detected from a northern latitude.

Through simulations (Giorgini et al., 2009; Naidu et al., 2016) it was concluded that there is a small, but non-zero, fraction of NEO's are not observable from the northern hemisphere.

Near Earth asteroid detection from southern hemisphere (Australia) since 2015

In 2015 the Southern Hemisphere Asteroid Radar Program (SHARP) (Benson et al., 2017) began its first radar observations using available antenna time on the 70 and 34 m beam waveguide antennas located at the Canberra Deep Space Communication Complex (CDSCC).

A Doppler compensated continuous wave signal was transmitted at near Earth asteroid targets at either 2.114 GHz (14.2 cm S band) or 7.15945 GHz (4.2 cm X band). Reflected echoes were received at the 64 m Parkes or 6 m × 22 m Australia Telescope Compact Array (ATCA) antennas at Narrabri Australia, depending upon schedule availability of these facilities.

The CDSCC antennas, Parkes and ATCA telescopes are not optimised for bistatic radar observations but are respectively used for deep space mission command, telemetry/ranging and radio astronomy. These facilities were however found to be adaptable (Abu Shaban. et al., 2018) for the opportunity of radar observations of NEAs. Table 1 shows a summary of some of the NEAs illuminated by the SHARP.

The first target for SHARP shown in Figure 1, was the asteroid 2005 UL5 selected for the GSSR at the time when SHARP entered its first check out phase. 2005 UL5 has an estimated diameter of 300 m determined from optical light curves and was observed at closest approach on 20th November 2015 at a range of 0.0153 au (5 LD or Lunar distances). 2005 UL5 was illuminated with a circularly
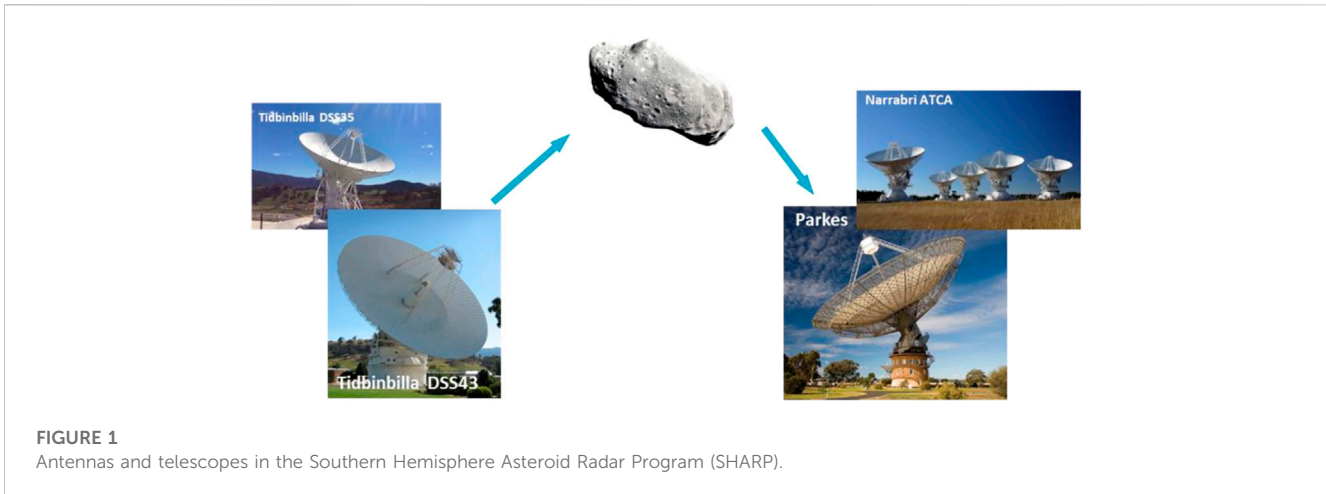
FIGURE 1
Antennas and telescopes in the Southern Hemisphere Asteroid Radar Program (SHARP).

TABLE 1 Selection of NEA targets illuminated by the SHARP 2015-2020 (15).

Asteroid	Class	Date	Approximate Diameter (m)	Range	Configuration DSS43 Tx with
2005 UL5	Aten	2015 Nov	250	6 LD	Parkes & ATCA
1998 WT24	Aten	2015 Dec	400	11 LD	Parkes & ATCA
3122 Florence	Amor	2017 Sep	5000	18 LD	ATCA
2012 TC4	Apollo	2017 Oct	10	0.1 LD	ATCA
2002 AJ129	Apollo	2018 Feb	700	10 LD	ATCA
2010 WC9	Apollo	2018 May	80	0.5 LD	ATCA
2003 SD220	Aten	2018 Dec	700	7 LD	ATCA
2019 EA2	Aten	2019 Mar	30	0.8 LD	ATCA
2019 GC6	Apollo	2019 Apr	20	0.5 LD	ATCA
2019 SP3	Apollo	2019 Oct	33	0.97 LD	ATCA
2020 SO	Artificial	2020 Nov	10	0.5 LD	ATCA
2020 XX3	Apollo	2020 Dec	7	0.15 LD	ATCA

polarised Doppler compensated transmission with centre frequency of 2.114 GHz by DSS-43, the 70 m antenna at CDSCC using 75 kW continuous RF power. 2005 UL5 echoes were received by the 64 m Parkes radio telescope with detections recorded in dual polarisations.

A second asteroid, 1998 WT24 was illuminated similarly during its closest approach to the Earth on 11th December 2015 at a range of 0.028 au (10.9 LD). 1998 WT24 is an asteroid of diameter 415 m. Approaching Earth from the south 1998 WT24 represented an example of how a southern hemisphere planetary radar capability could enable the earlier detection of NEOs.

With the success of two NEO observations, from 2015 to 2022 SHARP (Molyneux et al., 2019) has illuminated and tracked many NEOs ranging in diameter from 20m to 5000 m at ranges of 0.1–18 LD. This has shown the feasibility of NEO detection by a non-dedicated southern hemisphere capability located in Australia (CSIRO, 2021).

In March 2021, the University of Tasmania (UTAS) joined SHARP operations with the observation of asteroids and space debris. UTAS operates a continent-wide array of radio telescopes including three 12, a 26 m and a 30 m dishes. UTAS has conducted a total of 17 observations between 2021 and 2022. While the collecting area of the 12 m antennas is significantly smaller than ATCA or Parkes, the UTAS antennas offer diversity in geographic location and availability. Asteroid observations of 1994 PC1 and 2003 SDA have been achieved.

Augmentation of bistatic radar using small aperture optical telescopes

For many years northern hemisphere optical observatories (Catalina, Pan-STARRS, Atlas and Linear) (1) have tracked and observed asteroids effectively. A southern hemisphere widefield optical system such as at the Siding Spring Observatory has participated at times in NEO detection.
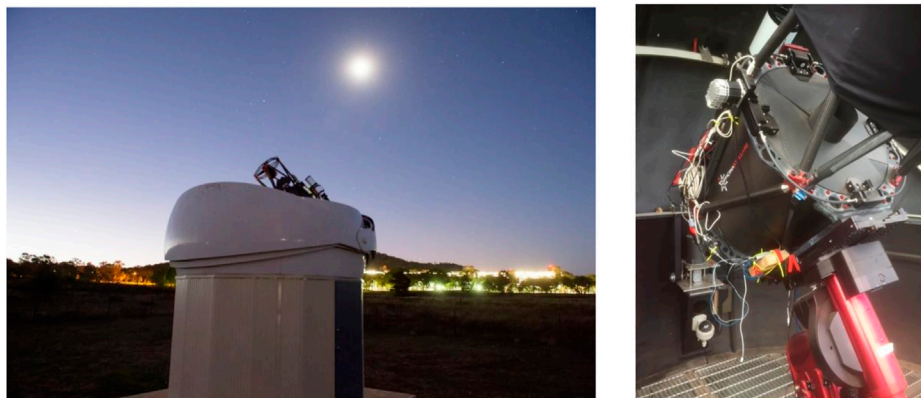
FIGURE 2
UNSW managed Falcon Telescope part of the USAFA Falcon Network.

TABLE 2 NEA targets illuminated by the SHARP 2022.

NEA	Class	Date (DOY)	Approx Diameter [m]	Range [LD]	SHARP Configuration	Abs Vis Mag	Optical Scope
2001 CB21	Apollo	4Mar 2022 (063)	500–1200	12.8	CDSCC-34 m Xband Tx/ ATCA Rx	18.5	Falcon 0.5 m (Clouded)
2008 AG33	Apollo	27Apr 2022 (117)	300–800	8.4	CDSCC-70 m Xband Tx/ ATCA Rx	19.4	Falcon 0.5 m Skynet 0.35 m & 0.4 m Perth
2012 UX68	Apollo	15May 2022 (135)	30–120	2.5	CDSCC-70 m Xband Tx/ ATCA Rx	24.2	Falcon 0.5 m (Clouded) NZ 0.35 m
1989 JA	Apollo	27-28 May 2022 (147-148)	1800	10.5	CDSCC-70 m Xband Tx/ ATCA Rx	17.8	Falcon 0.5 m incl. Spectroscopy
2022 LV	Apollo	25Jun 2022 (176)	20–40	2.0	CDSCC-70 m Xband Tx/ ATCA Rx	25.3	Magnitude beyond limits

The relocation of the 3.4 m DARPA Space Surveillance Telescope (SST) once located in the northern hemisphere at White Sands United States, to Exmouth in Western Australia, may hold further optical tracking options. In 2020 the NASA and US DoD signed an MOU related to the use of the SST for NEO observations (NASA, 2020). The SST was previously found to be very effective at NEO detection (Stuart et al., 2014).

In 2022 a program of augmenting bi-static radar observations using SHARP with rapidly acquirable sub-metre-class 0.3–0.5 m optical apertures began. Optical telescopes such as those managed by UNSW in Figure 2, observed the Apollo and Aten class NEO's shown in Table 2 because of their Earth orbit crossing nature and classification as potentially hazardous asteroids (PHAs).

UNSW manages two sub-metre class wide field optical telescopes (Falcon and Viper). The USAFA-led Falcon Telescope Network includes a node in Canberra operated by UNSW Canberra (Chun, 2018). The telescope, designed for Space Situational Awareness, is a 0.5 m f8.1 main telescope with a 4 m focal length. This is accompanied by an Astrotech AT106 0.1 m f6.5 refractive viewfinder telescope with focal length 690 mm. The main telescope is equipped with a standard filter wheel with common spectral filters and a 100 lp/mm diffraction grating for slit-less spectroscopy. The currently installed cameras on both telescopes are cooled, Atik 414ex (SONY ICX825 sensor with 1380 × 1040 6.46 μm square pixels) with an option to swap in a CeleX5 Event Based Image Sensor for high temporal rate observations. The pixel field of view from the main telescope is 1.6 μrad, and 6.5 μrad in the viewfinder. Observations can be automatically or manually operated.

The VIPER observatory (Spaceacademy, 2023) consists of a Celestron 0.36 m Rowe-Ackermann Schmidt Astrograph (f/2.2) on a Software Bisque "Paramount MX+" GEM robotic telescope mount. The detector is a Ximea CB120MG-CM-X8G3 monochrome CMOS camera, with a resolution of 4096 × 3072 pixels (12.5 Mpixels) and pixel scale of 1.44 arcsec/px, providing a wide field capture of over a degree of sky per frame. The camera is directly connected, via a high-speed PCIe bus, to an NVIDIA Jetson TX2 system on a chip (SOC) (mounted atop the optical telescope assembly), enabling the use of innovative AI-at-the- edge and GPU image processing algorithms.

Extended optical observations were also supported by the Skynet Telescope at Perth Observatory in Western Australia using a Celestron C-14 telescope (0.35 m) in sidereal track, through colleagues at the University of Western Australia (UWA). These
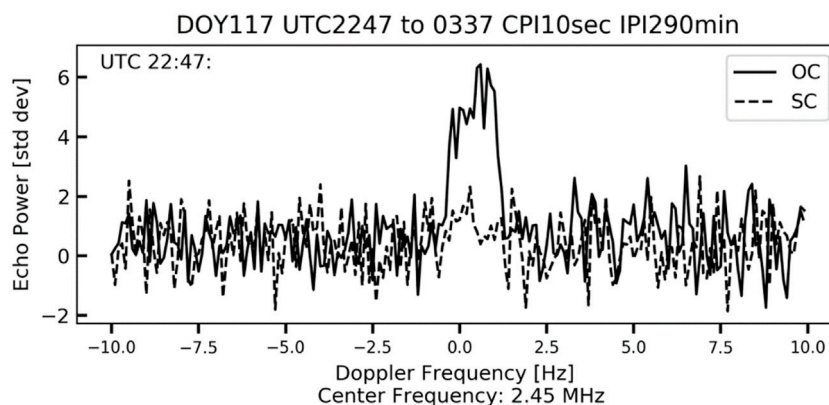
FIGURE 3
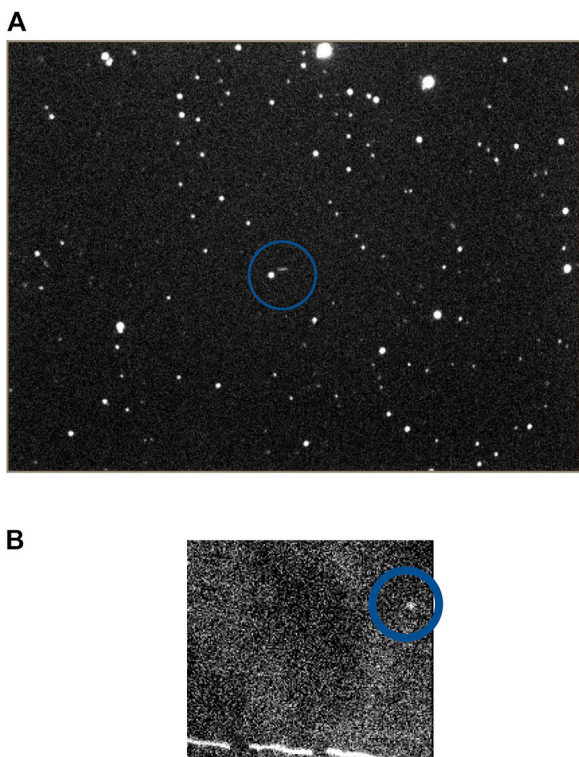Echo spectra for 2008 AG33 with CPI 10 s and IPI 290 min.

FIGURE 4
(A) Skynet Perth Observatory C-14 image tracking in sidereal mode and integrated for 120 s indicating asteroid 2008 AG33 streak at the predicted position centre of image (within the blue circle). **(B)** Falcon telescope image operating in rate-track mode captured a series of 200−300 s exposures, which are post-aligned to produce the detectable 2008 AG33 image.

were augmented by the 40 cm RCOS Skynet telescope at the Australian Space Academy site at Meckering WA.

We also include observers in New Zealand using a 0.35 m f11 telescope which added the value of geographic diversity and the utility of synchronised small agile optical telescopes to augment the SHARP bistatic radar.

Observations

During January to July 2022, the southern hemisphere asteroid radar program (SHARP) observed five NEO's together with the family of sub-metre optical telescopes indicated in Table 2.

Radar data was received as 8bit unsigned integers with the two polarisations (SC/OC) interleaved. To derive quantitative and qualitative information about the Asteroid's properties a Bistatic Long Baseline Array (LBA) processor coded in Python was utilised to produce echo power spectra. Data was analysed using the well known Radar Eq. 1 and the Doppler bandwidth Eq. 2 to determine NEA diameter, polarisation (SC/OC) ratio and rotational period.

$$P_{rx} = P_{tx}G_{tx}G_{rx}\lambda^2\sigma \left/ (4\pi)^3 R^4 \right. \qquad (1)$$

Where P_{rx} is the receive power, P_{tx} is the transmit power, G_{rx} is the receive antenna gain, G_{tx} is the transmitter antenna gain, λ is the radar wavelength, σ is the radar cross-section and R is the range.

$$B = 4\pi D(\phi)\cos(\delta) \left/ \lambda P_{rot} \right. \qquad (2)$$

where B is the Doppler bandwidth, $D(\phi)$ is the asteroid diameter in km at a phase of ϕ, $cos(\delta)$ is the sub-radar latitude, λ is the echo wavelength and P_{rot} is the asteroid rotational period (Ostro, 1993).

2001 CB21 bistatic radar configuration (DSS-36 Tx, ATCA Rx)

2001 CB21 orbits the Sun every 384 days (1.05 years), ranging between 0.69-1.38 AU from the Sun with an optically estimated diameter of 0.523-1.170 km (NASA, 2023a). 2001 CB21 was observed for 3 h during close approach on 4th March 2022 with SHARP using DSS-36 a 34 m CDSCC antenna transmitting at 20kW X band in Doppler compensated continuous wave mode and received at ATCA.Echo spectral data showed irregular data with significant variations in received power, a very narrow return and circular polarisation ratio of 1.1 suggesting possible data contamination with radio frequency interference (RFI). This observation was therefore discounted and not shown here. 2001 CB21 was also observed by the Falcon 0.5 m telescope but weather hindered any significant data capture.
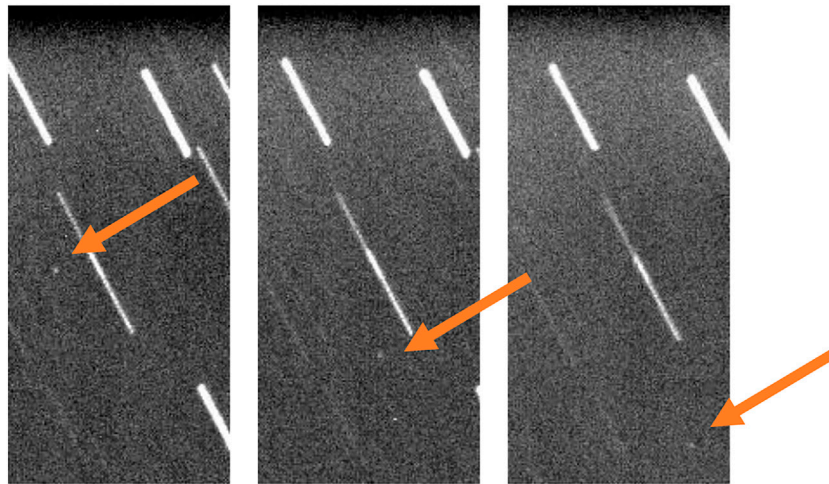
FIGURE 5
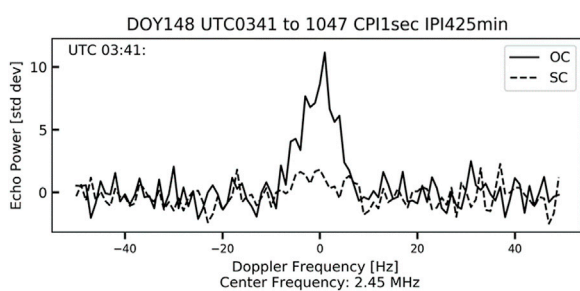Imagery of 2012 UX68 provided by astronomers in New Zealand using bracketed post-stacking of images.

FIGURE 6
Echo spectra for 1989 JA with CPI 1 s and IPI 425 min.

2008 AG33 bistatic radar configuration (DSS-43 Tx, ATCA Rx)

2008 AG33 orbits the Sun every 643.5 days (1.77 years), ranging between 0.97-1.95 AU from the Sun with an optically estimated diameter of between 0.35 and 0.79 km (NASA, 2023b). 2008 AG33 was observed for 5 h during close approach on 27th April 2022 with SHARP using DSS-43 the 70 m antenna at CDSCC at 20kW X band in Doppler compensated continuous wave mode and received by the ATCA.

An example of echo spectral data processed using a coherent integration period (CPI) of 10 s and non-coherent integration period (IPI) of 290 min is shown in Figure 3. With constant transmit power and synchronised reception, the echo spectra was found to vary over the observation period suggesting the rotation of a non-circular shaped asteroid. Calculations from the Doppler broadening indicate a diameter of $D = 630\ m \pm 140\ m$ and a circular polarisation ratio (SC/OC) of 0.3.

2008 AG33 optical

2008 AG33 was observed optically by the UNSW Falcon 0.5 m telescope and the Skynet C-14 Schmidt Cassegrain telescope at Perth Observatory. Poor weather in Canberra at the Falcon telescope delayed the observation by a day.

The Skynet Perth Observatory was able to observe on 4th May 2022, 1 week after SHARP observations. Operating in sidereal track mode, Figure 4A shows the C-14 image integrated for 120s, indicating the asteroid streak at the prescribed location centre of image. Figure 4B shows the (zoomed) stacked image from eight 200–300 s exposures of the NEO using rate-tracking based on an estimate of the coordinates of the NEO.

Post alignment and stacking was required to isolate the object given the error in the estimated position, tracking motion and actual survey coordinates. The limiting apparent magnitude of these observations is 17. Astrometric solutions used intervening 60 s exposures to limit the star trails.

2012 UX68 bistatic radar configuration (DSS-43 Tx, ATCA Rx)

2012 UX68 orbits the Sun every 415 days (1.14 years), ranging between 0.78-1.40 AU from the Sun with an optically estimated diameter of 0.026–0.118 km (NASA, 2023c). 2012 UX68 was predicted to be at closest approach on 15th May 2022 but with large positional uncertainties having not been observed for over a decade.

Due to these positional uncertainties, the pointing knowledge of SHARP and optical telescope was considered poor with az/el uncertainties of +/− 99°, with Doppler uncertainties of +/− 275 kHz, greatly exceeding the nominal Doppler compensation from the SHARP transmitter. It was therefore advised that recovery of 2012 UX68 should therefore be a task for an optical sweep sky survey.

2012 UX68 optical

The Falcon optical telescope planned to provide a sweep of the estimated position but was also not able to observe due to overcast and wet weather. Assistance was therefore requested from observers in New Zealand using a 0.35 m f11 telescope located near Mt John
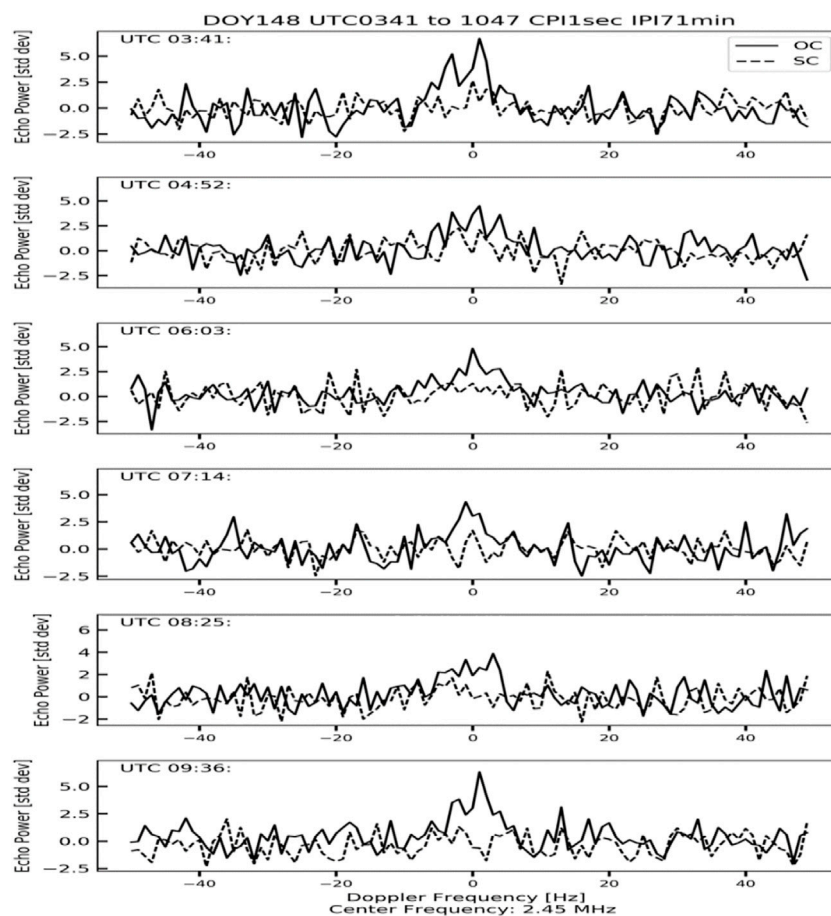
FIGURE 7
Six echo spectra of 1989 JA from 03:31 to 09:36 UTC DOY 148 each separated by 111 mins.

which had clear skies. Designated R57, the NZ telescope detected a NEA with consistent characteristics and positional data (Figure 5). JPL found that it was possible to link this to 2012 UX68 with a good fit.

Uncertainties for the new positional solution for 2012 UX68 were therefore significantly reduced to +/− 3 arcsec and +/− 6 Hz. This underscored the tasking agility, flexibility and value of small optical telescopes working directly with large aperture RF bi-static radar observations for NEA's to improve orbital location and therefore the PHA risk level.

1989 JA bistatic radar configuration (DSS-43 Tx, ATCA Rx)

1989 JA orbits the Sun every 862 days (2.36 years), ranging between 0.91 and 2.63 AU from the Sun with an original optically estimated diameter of 1.8 km (NASA, 2023d). 1989 JA was tracked over 2 days on the 27th/28th May with the longest track as 8 h. 1989 JA was calculated from data (example shown in Figure 6) to have a diameter of 624 m and an SC/OC ratio of 0.36. Diameter measurements from SHARP are smaller than the indicated optical estimates but nearer in consistency to the GSSR results of 680 m (NASA, 2023c).

Results from (NASA, 2023c) indicate that 1989 JA is also orbited by a Moon with period of 17.4 h. Figure 7 shows six echo spectra recorded from 03:31 to 09:36 UTC DOY 148 each separated by 111mins. Whilst there is noise in the spectra, there may be subjective evidence of a small peak moving left to right. Whether this is indicative of a Moon is unclear from our data but warrants the application of further research methods (e.g., advanced polarimetry).

1989 JA optical

1989 JA is sufficiently close and large that several optical photometric and spectroscopic techniques were able to be employed. The Falcon main telescope is equipped with a 100 lp/mm grating to allow for slitless spectroscopy, where the zero-order carries the actual image of each object and the first-order of the grating diffraction spreads the spectrum over the sparse extent of the sensor. Sometimes intervening objects occupy the pixels hosting first-order signal, but largely the spectrum (which should be a masked version of our own Sun's spectrum) is discernible. Photometric Sloan filters can be alternatively used in the B,V,R,I′,r′ g′, and z′ areas of the spectrum (Chun, 2018). The viewfinder acts as a companion recording the full spectrum allowed by the Si detectors.
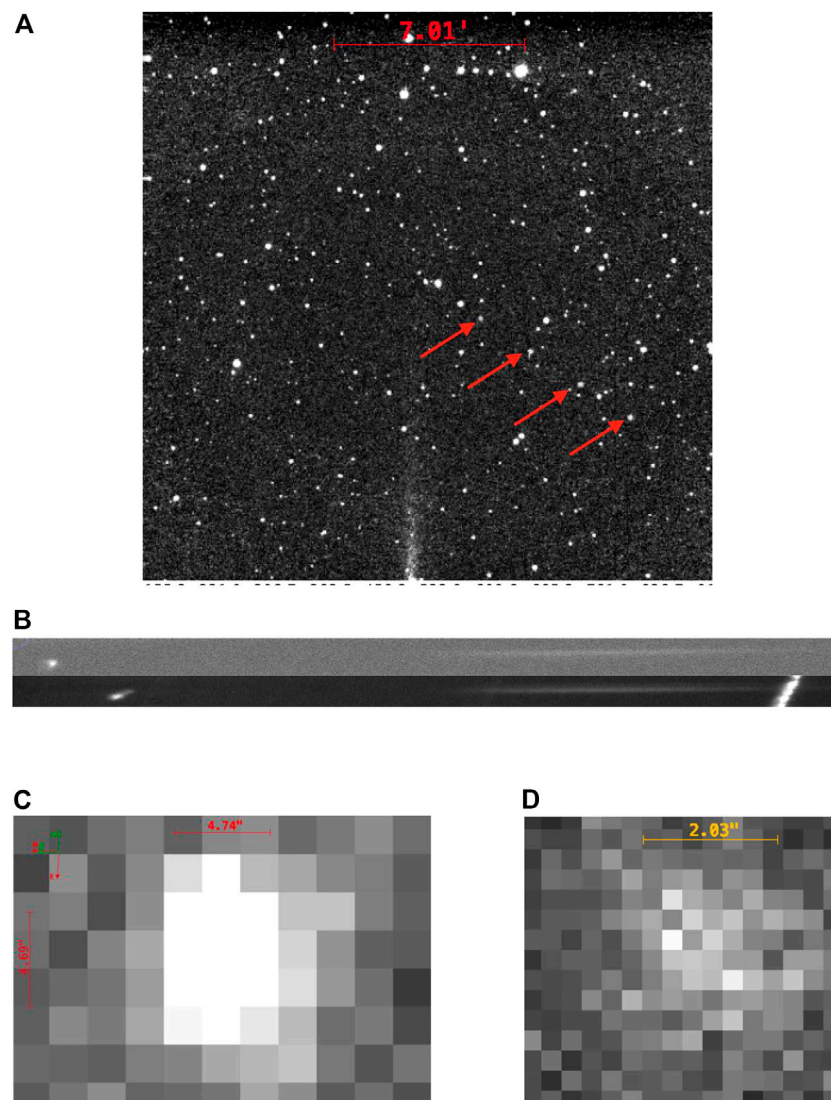
FIGURE 8
Optical Observations of 1989 JA. **(A)** Composite of images provided by the New Zealand Astronomers **(B)** slitless spectroscopic image from 1 s exposure from Falcon, and, the zoomed object detection in single 1 s exposure and frame averaged result from 1989 JA in the **(C)** Falcon viewfinder and **(D)** main telescope (R filter), indicating (seeing reduced) precision provided by optical telescopes.

Figure 8 illustrates the spectrum reflected by 1989 JA. We expect in a similar way to engage polarimetric observations in the future with such detectable targets. Figures 8C, D give an indication of the almost sub-arcsecond precision using modest optical telescopes.

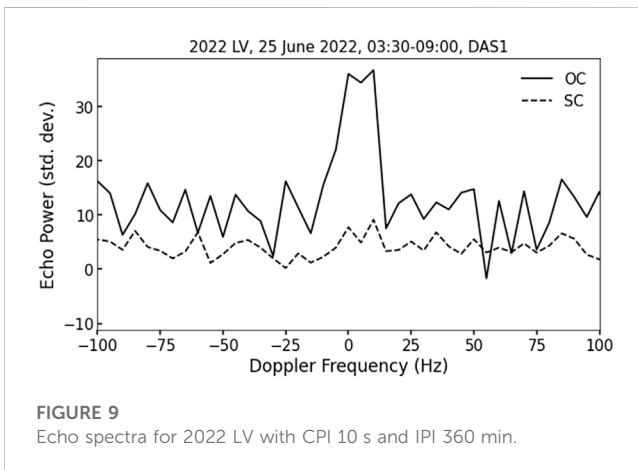## 2022 LV bistatic radar configuration (DSS-43 Tx, ATCA Rx)

2022 LV orbits the Sun every 452 days (1.24 years), ranging between 0.98 and 1.33 AU from the Sun with an optically estimated diameter of 0.017–0.038 km (Spacereference, 2022). 2022LV was observed on 25th and 26th June 2022 for 6hrs using the SHARP DSS-43 to ATCA configuration. Echo spectra shown in Figure 9, were found to be relatively constant over the observing period. Calculations indicate an asteroid diameter of D = 19.8 ± 1.8 m. 2022LV data presented a circular polarisation ratio (SC/OC) of 0.22.

2022 LV optical

The indicative magnitude 26 for 2022 LV indicated that optical observations with the sub metre optical telescopes described were unlikely to be successful for observing 2022 LV however attempts were made rate-tracking with the Falcon telescope with a potential object detected (Figure 10).

Summary and future work for southern hemisphere (Australian) NEO observations

Space debris comes in many forms and many locations in space. We often think about space debris in terms of near Earth human made objects, however in this article we indicate that Apollo and Aten class asteroids represent another form of space debris of a potentially hazardous nature to orbiting spacecraft and/or Earth

FIGURE 9
Echo spectra for 2022 LV with CPI 10 s and IPI 360 min.

FIGURE 10
2022 LV was rate-tracked with 100 s exposures. This is the sum of 56 frames, with a potential but unconfirmed candidate shown by the arrow.

based locations. We also show some of the operational challenges, types of facilities and the importance of geographic diversity necessary for detecting, observing and characterising asteroids, especially PHA's.

The SHARP bistatic radar program combined with small optical telescopes optical provides additional information on the characteristics of NEO's. We found that when the NEO was well known in orbital position, radar observations from SHARP could be used to refine astrometry, indicate diameter, polarization ratio and infer rotation. Where NEO positions presented with large uncertainties (e.g., 2008 UX68), we showed that the use of a small aperture optical telescope allowed a rapid local sky survey to re-discover and update the NEO orbital position with much improved uncertainty.

Leveraging the progress from the NEO campaign in the first half of 2022, we propose continuing with SHARP observations over the next few years including:

- Future NEO target planning for radar bistatic and small optical telescopes
- Development of Stokes Vector Analysis with existing radar bistatic NEO data
- Testing new optical sensors including Event Based Systems (EBS)
- Translation of NEO target interpretations to human made objects

Asteroid class and composition have been shown to be correlated to circular polarisation ratios (Benner et al., 2008) and leads to insights related to the formation and histories of the object. Advanced polarimetry using Stokes vector decomposition has resulted in further characterisation of physical properties including shape (Sriram and Anne, 2019), ice content (Black, 2001), surface roughness (e.g., boulders) and viewing geometry (Hickson et al., 2021). Stokes parameters provide an alternative description of the polarisation state of NEO echoes and is experimentally convenient because each parameter corresponds to a sum or difference of measurable complex values. We propose to examine the values of I, Q, U and V polarisation properties and attempt to compare to NEO characteristics including surface characteristics, spin state, surface materials and
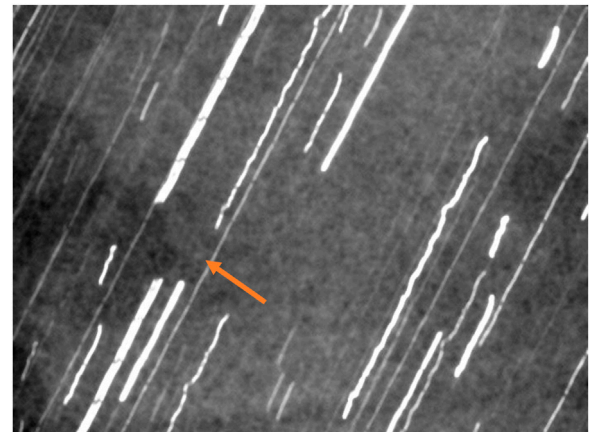
ice content. The feasibility of this type of research has been considered (Wang et al., 2015) with promising results.

Using elements of the above Stokes vector NEO analysis, the translation of NEO target interpretations to human made objects for deep space objects, could be approached similarly. Human made objects are likely to display shape geometries far more angular than NEO's. Here the use of characteristic waterfall diagram analysis of the radar crossection, target doppler history and the ratio of opposite to same sense polarisation ratio (Rajan, 2016) could be early markers for discrimation of the size, shape, material and spin of human made objects (Adsabs, 2021; NASA, 2021).

Data availability statement

The original contributions presented in the study are included in the article/supplementary material, further inquiries can be directed to the corresponding author.

Author contributions

EK is the corresponding author and paper writer, EK collated RF and optical data from co-authors and provided student support. LB provided paper oversight and expert RF opinion. RB provided UNSW resources, MB provided expert opinion, SD provided RF data analysis, PE provided expert opinion, JG provided ephermis and pointing data, SH established RF telescope access and took raw RF data and per-analysed, AL collected optical data and provided expert opinion, JL provided expert opinion and resources, EP provided student guidance and expert opinion, CP provided RF access and expert opinion. JS provided RF access and expert opinion. All authors contributed to the article and approved the submitted version.

Funding

Acknowledgments

Conflict of interest

The authors declare that the research was conducted in the absence of any commercial or financial relationships that could be construed as a potential conflict of interest.

Publisher's note

All claims expressed in this article are solely those of the authors and do not necessarily represent those of their affiliated organizations, or those of the publisher, the editors and the reviewers. Any product that may be evaluated in this article, or claim that may be made by its manufacturer, is not guaranteed or endorsed by the publisher.

References

Abu Shaban, Z., Benner, L., Edwards, L., Lazio, J., Stevens, J., Boyce, R., et al. (2018). Asteroid observations from the southern hemisphere using planetary radar. J. 42nd COSPAR Sci. Assem. 1-79–18.

Adsabs (2021). Study of the asteroid florence. https://ui.adsabs.harvard.edu/abs/2021DPS 5340406L/abstract.

Benner, L. M., Ostro, S. J., Magri, C., Nolan, M. C., Howell, E. S., Giorgini, J. D., et al. (2008). Near-Earth asteroid surface roughness depends on compositional class. Icarus 198, 294–304. doi:10.1016/j.icarus.2008.06.010

Benson, C., Reynolds, J., Stacy, N., Benner, L., Edwards, P., Baines, G., et al. (2017). First detection of two near Earth asteroids with a southern hemisphere planetary radar system. J. Radio Sci., 52 (11), 1344–1351.

Black, G. (2001). Icy galilean satellites: Modelling radar reflectivities as a coherent backscatter effect. Icarus 151, 167–180. doi:10.1006/icar.2001.6616

Chun, F. K. (2018). The Falcon telescope Network. Publ. Astronomical Soc. Pac. 130 (991), 095003.

CSIRO (2021). Southern hemisphere asteroid radar. Present. by Emi Cashman ANU student intern CSIRO.

Giorgini, J. D., Chodas, P. W., Slade, M. A., Preston, R. A., and Yeomans, D. K. (2008). "DSN radar upgrade study," in Jet propulsion laboratory (Pasadena, CA, USA: National Aeronautics and 350 Space Administration).

Giorgini, J. D., Slade, M. A., Silva, A., Preston, R. A., Brozovic, M., Taylor, P. A., et al. (2009). "Improved impact hazard assessment with existing radar sites and a new 70-m southern hemisphere radar installation," in Jet propulsion laboratory (Pasadena, CA, USA: National Aeronautics and Space Administration). http://hdl.handle.net/2014/45220.Radar Astrometry of Small Bodies: Detection, Characterization, Trajectory Prediction, and Hazard Assessment," Giorgini, J. D., et al. 2009, White Paper, submitted to the Planetary Sciences Decadal Survey (2013–2022); http://www.lpi.usra.edu/decadal/sbag/topical wp/JonDGiorgini.pdf and https://trs.jpl.nasa.gov/handle/2014/45703

Hickson, D. C., Virkki, A. K., Perillat, P., Nolan, M. C., and Bhiravarasu, S. S. (2021). Polarimetric decomposition of near-earth asteroids using Arecibo radar observations. Planet. Sci. J. 2, 2632–3338. doi:10.3847/PSJ/abd846

Molyneux, B., Horiuchi, S., Stevens, J., Baines, G., Benson, C., Abu Shaban, Z., et al. "Southern hemisphere asteroid program (SHARP): Targets of opportunity observations of near Earth asteroids 2019 EA2, 2019 GC6, 2019 SP3," in Proceedins of the 43rd COSPAR Scientific Assembly, Sydney Australia, January 2021.

Muhleman, D. O., Butler, B. J., Grossman, A. W., and Slade, M. A. (1991). Radar images of Mars. Science 253, 1508–1513. doi:10.1126/science.253.5027.1508

Muhleman, D. O., Grossman, A. W., Butler, B. J., and Slade, M. A. (1990). Radar reflectivity of titan. Science 248, 975. doi:10.1126/science.248.4958.9

Naidu, S. P., Benner, L. A. M., Margot, J.-L., Busch, M. W., and Taylor, P. A. (2016). Capabilities of Earth-based radar facilities for near-Earth asteroid observations. https://arxiv.org/abs/1604.01080.

NASA (2023d). Goldstone radar observations planning. https://echo.jpl.nasa.gov/asteroids/1989JA/1989JA.2022.goldstone.planning.html.

NASA (2020). Memorandum of agreement (MOA) entered into between HQ USSF/S5/9 and NASA/SMD. https://www.nasa.gov/saa/domestic/32284_USSF_59_NASA_SMD_SST_Data_MOA_Final_fullysigned.pdf.

NASA (2021). Near-earth object observations program. https://www.nasa.gov/planetarydefense/neoo.

NASA (2023a). Small-body database lookup. https://ssd.jpl.nasa.gov/tools/sbdb_lookup.html#/?sstr=2001%20CB21.

NASA (2023b). Small-body database lookup. https://ssd.jpl.nasa.gov/tools/sbdb_lookup.html#/?sstr=2008%20AG33.

NASA (2023). Small-body database lookup. https://ssd.jpl.nasa.gov/tools/sbdb_lookup.html#/?sstr=2012%20UX68.

Ostro, S. J. (2007). "Planetary radar," in Encyclopedia of the solar system, 2 nd 372 edition. Editors L. A. McFadden, P. R. Weissman, and T. V. Johnson (Cambridge, Massachusetts, United States: Academic Press), 735–374.

Ostro, S. J., and Giorgini, J. D. (2004). "The role of radar in predicting and preventing asteroid and comet collisions with Earth," in Mitigation of hazardous comets and asteroids (Cambridge, United Kingdom: Cambridge University Press), 38.

Ostro, S. J., and Pettengill, G. H. (1978). Icy craters on the Galilean satellites. Icarus 34, 378–268. doi:10.1016/0019-1035(78)90167-7

Ostro, S. J. (1993). Planetary radar astronomy. Rev. Mod. Phys. 65, 1235–1279. doi:10.1103/RevModPhys.65.1235

Rajan, N. (2016). Orbital debris size estimation from radar cross section measurements. https://conference.sdo.esoc.esa.int/proceedings/sdc3/paper/17/SDC3-paper127.pdf.

Slade, M. A., Butler, B. J., and Muhleman, D. O. (1992). Mercury radar imaging: Evidence for polar ice. Science 258, 635–640. doi:10.1126/science.258.5082.635

Spaceacademy (2023). Description of viper 0.4m telescope (private communication with dr lauren glina). Available at, http://www.spaceacademy.net.au/asa/skynet/skynet.htm.

Spacereference (2022). Apollo-class asteroids. https://www.spacereference.org/asteroid/2022-lv.

Sriram, S. B., and Anne, K. V. (2019). Modeling radar albedos of laboratory-characterized particles: Application to the lunar surface. J. Geophys. Res. Planets 124, 3025–3040. doi:10.1029/2019JE006006

Stuart, J. S., Freedman, D., Ronak, W., Shah, R. Y., and Shah, Y. (2014). Detecting small asteroids with the space surveillance telescope. Icarus 239, 253–259. doi:10.1016/j.icarus.2014.06.012

Wang, H., Zhou, Z., Turnbull, J., Song, Q., and Qi, F. (2015). Three-component decomposition based on Stokes vector for Compact polarimetric SAR. Sensors 15, 24087–24108. doi:10.3390/s150924087